Science Advances
AAAS

advances.sciencemag.org/cgi/content/full/5/8/eaaw6081/DC1

Supplementary Materials for

Engineered collagen-binding serum albumin as a drug conjugate carrier for cancer therapy

Koichi Sasaki, Jun Ishihara, Ako Ishihara, Risako Miura, Aslan Mansurov, Kazuto Fukunaga, Jeffrey A. Hubbell*

*Corresponding author. Email: jhubbell@uchicago.edu

Published 14 August 2019, *Sci. Adv.* **5**, eaaw6081 (2019)
DOI: 10.1126/sciadv.aaw6081

This PDF file includes:

Fig. S1. Confirmation of CBD fusion to SA by MALDI-TOF MS analysis.
Fig. S2. Binding affinities of CBD-SA to collagen type I and type III.
Fig. S3. SDS-PAGE analysis of mouse SA and CBD-SA conjugated with Dox.
Fig. S4. Hydrodynamic sizes.
Fig. S5. The binding interface between collagen type III and A3 domain of VWF.
Fig. S6. In vitro release kinetics of Dox from Dox-SA.
Fig. S7. Plasma pharmacokinetics of DyLight 800–labeled SA and CBD-SA.
Fig. S8. Changes of hematological values in mice receiving aldoxorubicin or Dox-CBD-SA (20 mg/kg).
Fig. S9. Histological analysis of major organs after Dox-CBD-SA treatment.
Fig. S10. MC38 tumor rechallenge and body weight changes of MC38 tumor-bearing mice during the treatment.
Table S1. Amino acid sequence of CBD-SA.

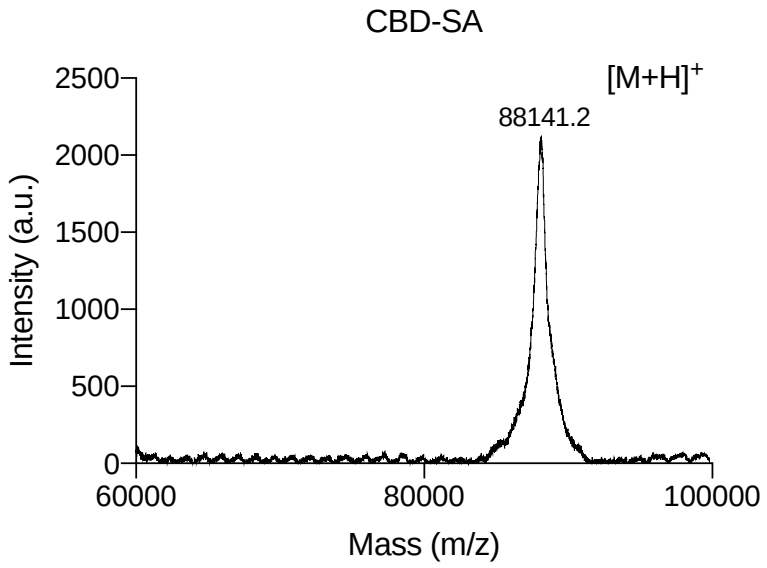

Fig. S1. Confirmation of CBD fusion to SA by MALDI-TOF MS analysis. CBD-SA was analyzed by MALDI-TOF MS. Abscissa is mass to charge ratio (m/z) and ordinate is intensity of charged ions. Two experimental replicates.

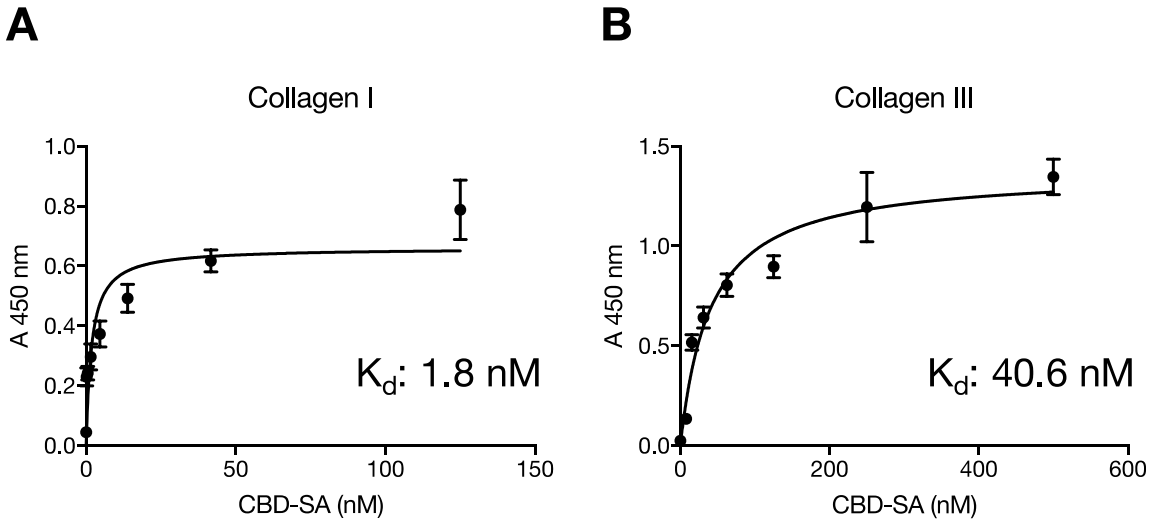

Fig. S2. Binding affinities of CBD-SA to collagen type I and type III. Affinities of CBD-SA against (A) collagen type I and (B) collagen type III were determined by ELISA (n = 4, mean ± SD). Graphs with [concentrations] vs [signals] are shown. Two experimental replicates.

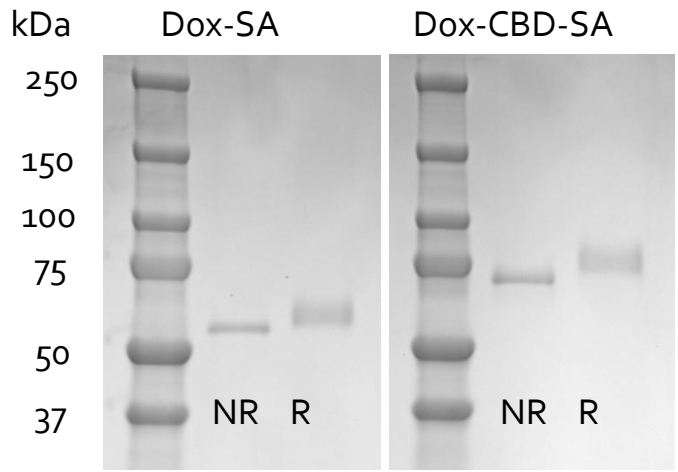

Fig. S3. SDS-PAGE analysis of mouse SA and CBD-SA conjugated with Dox. Dox-SA and Dox-CBD-SA were analyzed by SDS-PAGE with coomassie blue staining. R reduced; NR non-reduced. Representative images are presented. Two experimental replicates.

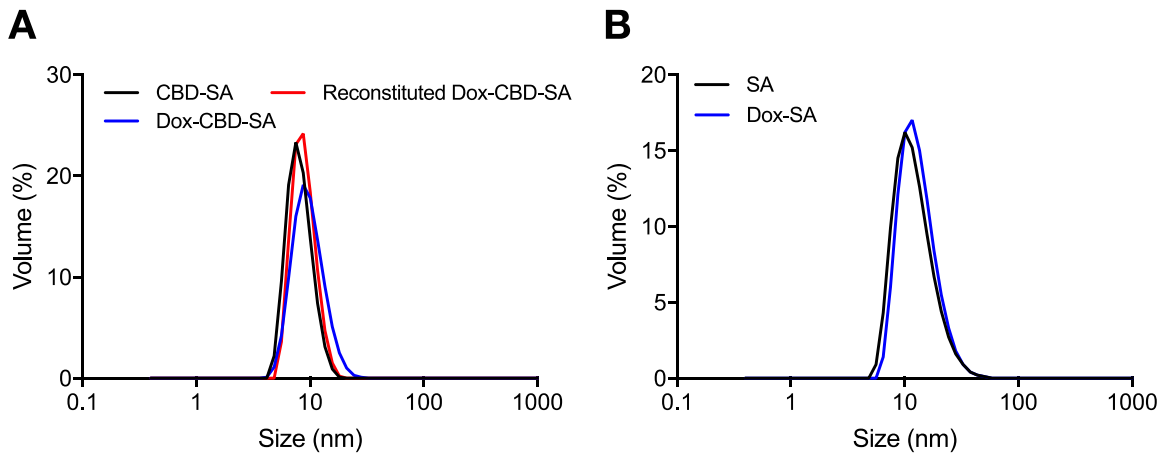

Fig. S4. Hydrodynamic sizes. (A) Sizes of un-conjugated CBD-SA, Dox-CBD-SA and Dox-CBD-SA reconstituted after lyophilization were measured by DLS. (B) Sizes of un-conjugated SA and Dox-SA were also measured. Two experimental replicates.

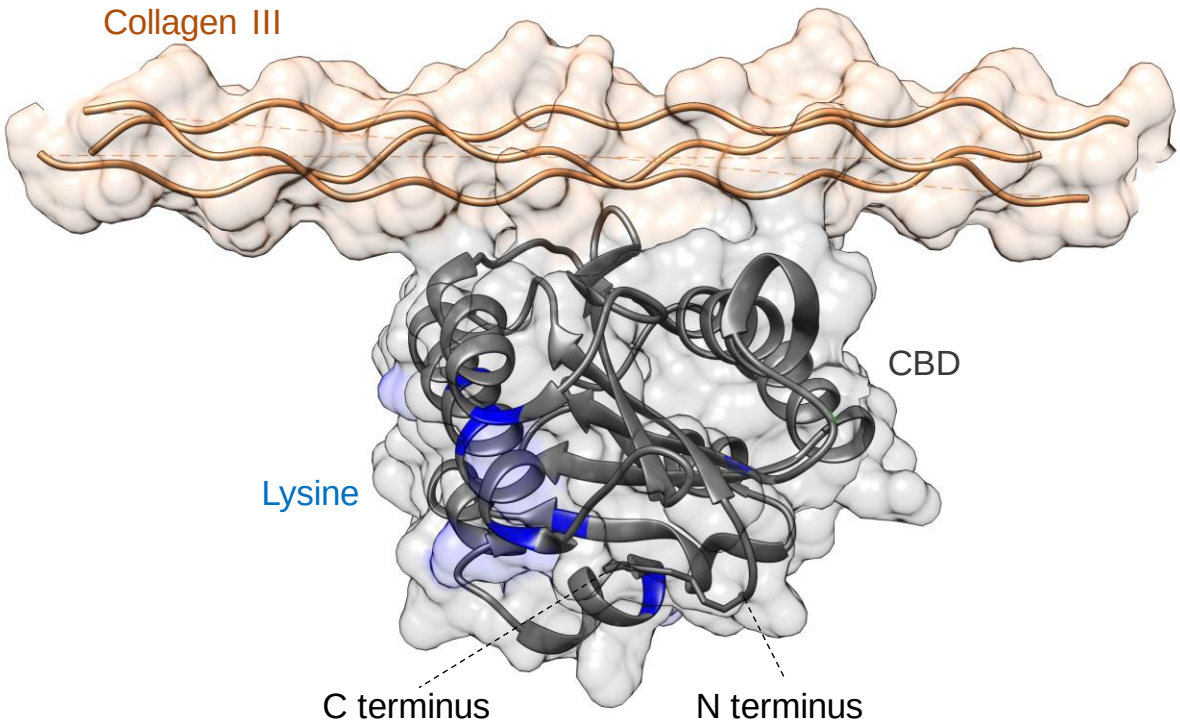

Fig. S5. The binding interface between collagen type III and A3 domain of VWF. Crystal structure of the A3 domain of von Willebrand factor (CBD) in complex with type III collagen (PDB 4DMU). The Image was processed using UCSF chimera. Lysines are indicated as blue color.

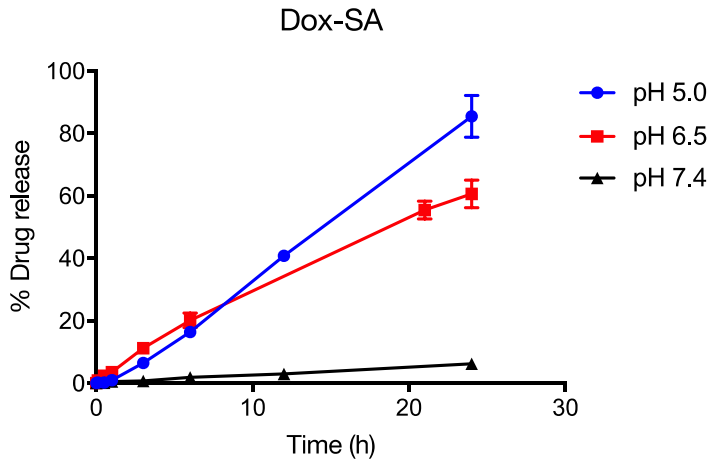

Fig. S6. In vitro release kinetics of Dox from Dox-SA. Dox release kinetics from Dox-SA under three different pH conditions were evaluated by fluorescence (excitation at 495 nm, emission at 590 nm, n = 3, mean ± SD). Two experimental replicates.

A

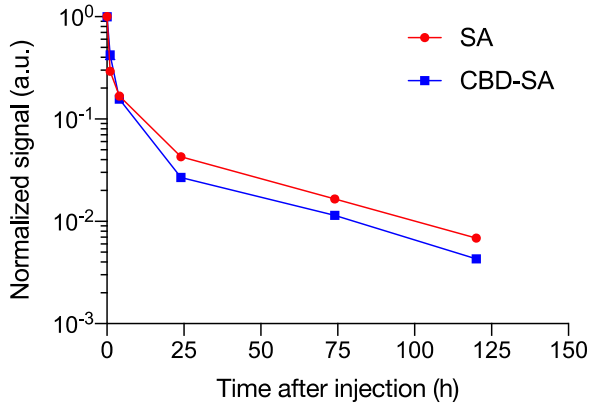

B

	$t_{½, β}$ (h)
SA	8.9 ± 1.6
CBD-SA	7.3 ± 1.0

Fig. S7. Plasma pharmacokinetics of DyLight 800–labeled SA and CBD-SA. 200 μg of DyLight 800 labeled SA or CBD-SA were administered to tumor-free FVB mice via tail vein injection (i.v.). Blood plasma was collected at indicated time points. (A) Signal intensity of each sample was normalized with mean signal intensity of samples collected at 1 min after injection (mean ± SEM, n = 4). (B) Plasma half-lives of labeled SA and CBD-SA were calculated using two-phase exponential decay: MFI (t) = $Ae^{-\alpha t} + Be^{-\beta t}$. $t_{½, β}$, slow clearance half-life. (mean ± SEM. n = 4). One experimental replicate.

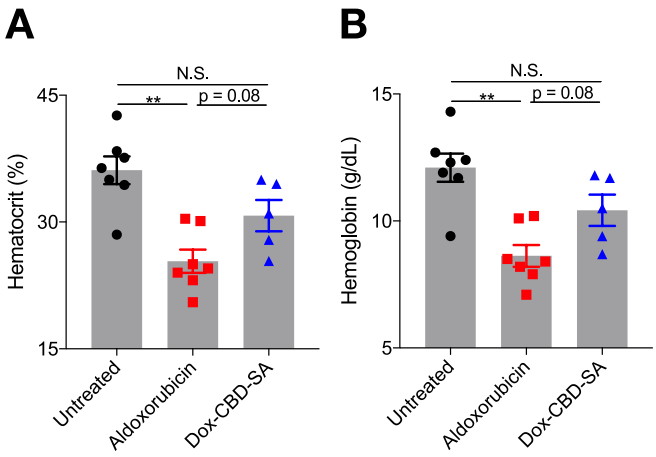

Fig. S8. Changes of hematological values in mice receiving aldoxorubicin or Dox-CBD-SA (20 mg/kg). (A) Hematocrit and (B) hemoglobin concentration on day 6 after injection. Two experimental replicates. Statistical analyses were done using ANOVA with Tukey's test. **p < 0.01; N.S. = not significant.

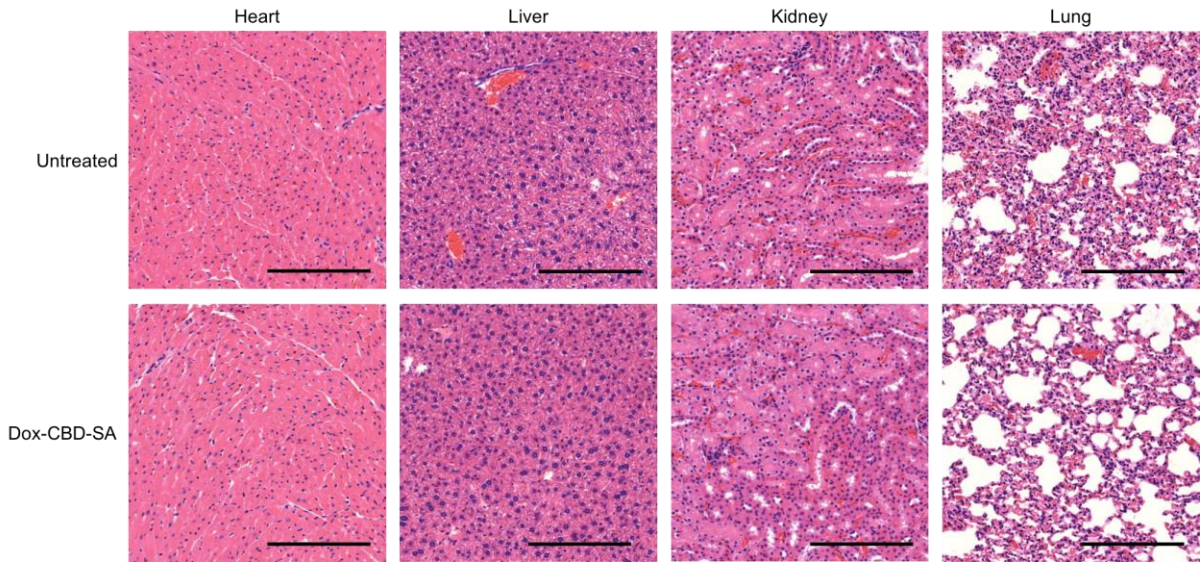

Fig. S9. Histological analysis of major organs after Dox-CBD-SA treatment. Tumor-free FVB mice received Dox-CBD-SA (20 mg/kg) on day 0. On day 16, heart, liver, kidney, and lung were harvested and processed to obtain histologic sections (n = 7 for untreated, n = 5 for Dox-CBD-SA). Scale bar = 200 μm. H&E stained histology was evaluated blindly and no significant abnormality was observed after Dox-CBD-SA treatment. Representative images are shown. Two experimental replicates.

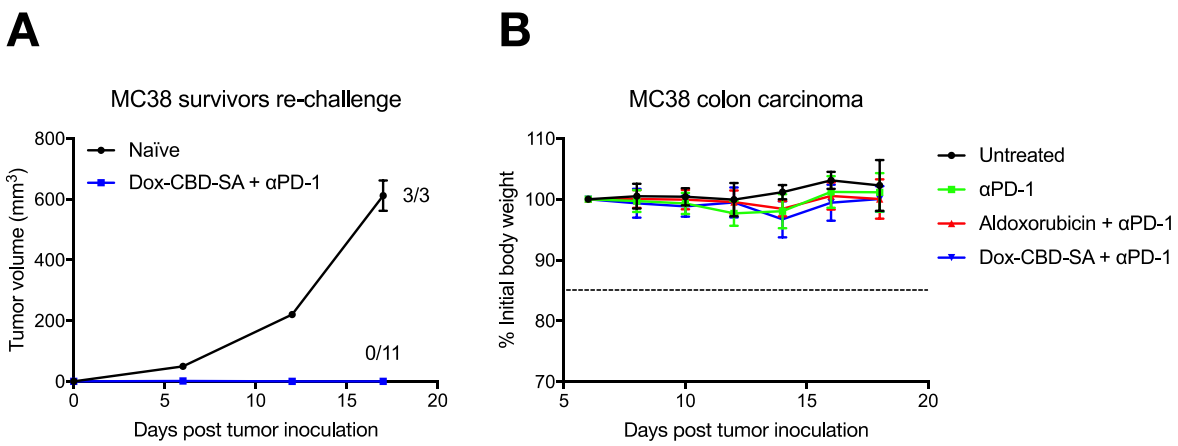

Fig. S10. MC38 tumor rechallenge and body weight changes of MC38 tumor-bearing mice during the treatment. (A) Graph depicts tumor sizes of Dox-CBD-SA + αPD-1 treated survivors re-challenged with MC38 cells (mean ± SEM). Naïve mice were also challenged with the same amounts of cells as a control group. # of mice developed a palpable tumor is shown. (B) Body weight changes of mice during the treatments in Fig. 5 (mean ± SEM). A line represents 85% of initial body weight. Two experimental replicates.

Table S1. Amino acid sequence of CBD-SA. VWF A3 domain and mouse SA

CSQPLDVILLLDGSSSFPAS
YFDEMKSFAKAFISKANIGP
RLTQVSVLQYGSITTIDVPW
NVVPEKAHLLSLVDVMQREG
GPSQIGDALGFAVRYLTSEM
HGARPGASKAVVILVTDVSV
DSVDAAADAARSNRVTVFPI
GIGDRYDAAQLRILAGPAGD
SNVVKLQRIEDLPTMVTLGN
SFLHKLCSGFVRIGGGSGGG
SEAHKSEIAHRYNDLGEQHF
KGLVLIAFSQYLQKCSYDEH
AKLVQEVTDFAKTCVADESA
ANCDKSLHTLFGDKLCAIPN
LRENYGELADCCTKQEPERN
ECFLQHKDDNPSLPPFERPE
AEAMCTSFKENPTTFMGHYL
HEVARRHPYFYAPELLYYAE
QYNEILTQCCAEADKESCLT
PKLDGVKEKALVSSVRQRMK
CSSMQKFGERAFKAWAVARL
SQTFPNADFAEITKLATDLT
KVNKECCHGDLLECADDRAE
LAKYMCENQATISSKLQTCC
DKPLLKKAHCLSEVEHDTMP
ADLPAIAADFVEDQEVCKNY
AEAKDVFLGTFLYEYSRRHP
DYSVSLLLRLAKKYEATLEK
CCAEANPPACYGTVLAEFQP
LVEEPKNLVKTNCDLYEKLG
EYGFQNAILVRYTQKAPQVS
TPTLVEAARNLGRVGTKCCT

LPEDQRLPCVEDYLSAILNR

VCLLHEKTPVSEHVTKCCSG

SLVERRPCFSALTVDETYVP

KEFKAETFTFHSDICTLPEK

EKQIKKQTALAELVKHKPKA

TAEQLKTVMDDFAQFLDTCC

KAADKDTCFSTEGPNLVTRC

KDALAHHHHHH